ADVANCED MATERIALS

Supporting Information

for *Adv. Mater.*, DOI: 10.1002/adma.201704028

A New 3D Printing Strategy by Harnessing Deformation, Instability, and Fracture of Viscoelastic Inks

*Hyunwoo Yuk and Xuanhe Zhao**

Supporting Information

A New 3D Printing Strategy by Harnessing Deformation, Instability, and Fracture of Viscoelastic Inks

Hyunwoo Yuk and Xuanhe Zhao

Effect of gravitational stretching and inertia

When the viscoelastic ink is extruded from the nozzle at H, the gravitational stretching of the printed fiber can be evaluated by the characteristic height which is defined as $H_{vg} \equiv \left(\frac{\eta_0 Q}{\rho g}\right)^{1/4}$, where η_0 is the zero-shear viscosity, $Q = \pi C(\alpha D)^2/4$ is the extrusion rate, ρ is the ink density, and g is the gravitation acceleration, respectively.[1] Since DIW 3D printing typically adopts relatively small H^* as printing parameter, the gravitational stretching is oftentimes negligible for highly viscoelastic inks. For example, the silicone elastomer ink properties and printing conditions used in this study (i.e., η_0 = 47,891 Pa·s, ρ = 1,105 kg·m^{-3}, g = 9.81 m·s^{-2}, and C = 450 mm·s^{-1}) gives $H_{vg} \approx 20H^*$ for D = 50 μm to 400 μm. Hence, the gravitational stretching is negligible in the range of H^* used in this study ($H^* \leq 10$). In addition, the rheological properties of viscoelastic inks in DIW 3D printing such as yield stress flow can further decrease the effect of gravitational stretching (**Figure S1c**). Hence, the diameter of printed fiber is nearly the same until it is deposited on the substrate or printed layer (**Figure S2a**). Under such condition, the inertial effect from the gravitational stretching is negligible.[1] Also, the nozzle tip moves with a constant speed without acceleration in this study. Therefore, the inertial effect in general can be regarded as negligible.

Condition for fracture of stretching viscoelastic ink

Stretching the extruded ink can significantly reduce the diameter of printed fibers and enhance the resolution of printing, until the ink fractures into discontinuous segments (**Figure S4a**).[2] Recent studies on the elastic fracture of viscoelastic liquids[3] have shown that the fracture of viscoelastic liquids occurs around a certain constant true strain over wide range of true strain rate when $Wi > 1$, where Wi is the Weissenberg number defined as $Wi \equiv \tau_{max}\dot{\varepsilon}$, with τ_{max} is the maximum relaxation time of viscoelastic liquid and $\dot{\varepsilon}$ is true strain rate of the stretching viscoelastic liquid. Hence, the boundary between thinning and discontinuous mode is $\varepsilon = \varepsilon_f$, where ε_f is true strain at fracture, given $Wi > 1$ during the discontinuous mode of printing. This boundary can also be expressed as $V^* = V_f^*$ by converting true strain into the corresponding non-dimensional nozzle speed. For the silicone elastomer ink used in this study, the experimental data show nearly constant value for ε_f (and corresponding V_f^*) with $Wi > 1$, exhibiting a good agreement with the condition for fracture of stretching viscoelastic ink (**Figure S4b** and **c**).

Additional References

[1] a) N. M. Ribe, *Proc. R. Soc. London, Ser. A* **2004**, *460*, 3223; b) N. M. Ribe, M. Habibi, D. Bonn, *Annu. Rev. Fluid Mech.* **2012**, *44*, 249.

[2] a) A. Y. Malkin, C. Petrie, *J. Rheol.* **1997**, *41*, 1; b) V. Barroso, R. Andrade, J. Maia, *J. Rheol.* **2010**, *54*, 605.

[3] a) H. Tabuteau, S. Mora, G. Porte, M. Abkarian, C. Ligoure, *Phys. Rev. Lett.* **2009**, *102*, 155501; b) Q. Huang, N. J. Alvarez, A. Shabbir, O. Hassager, *Phys. Rev. Lett.* **2016**, *117*, 087801; c) Q. Huang, O. Hassager, *Soft Matter* **2017**, *13*, 3470.

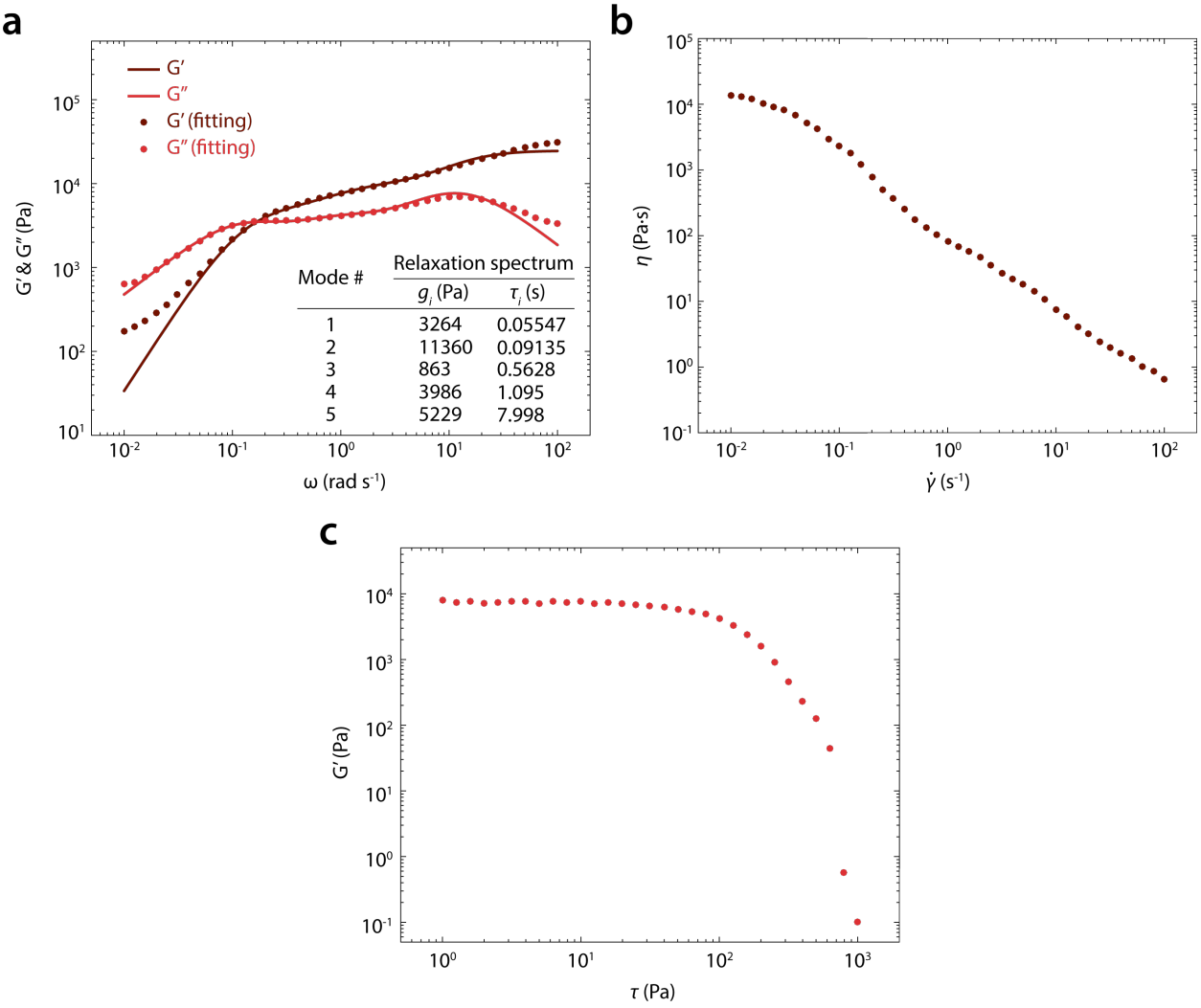

Figure S1. Rheological characteristics of the viscoelastic ink. a) Plot of storage modulus G' and loss modulus G'' as a function of angular frequency ω. The data are fitted with 5 modes Maxwell model with the listed relaxation spectrum. b) Plot of apparent steady-state viscosity η as a function of shear strain rate $\dot{\gamma}$. The viscoelastic ink exhibits a shear-thinning. c) Plot of G' as a function of shear stress τ. The viscoelastic ink exhibits a yield stress flow. All data were collected for room temperature (25 ℃).

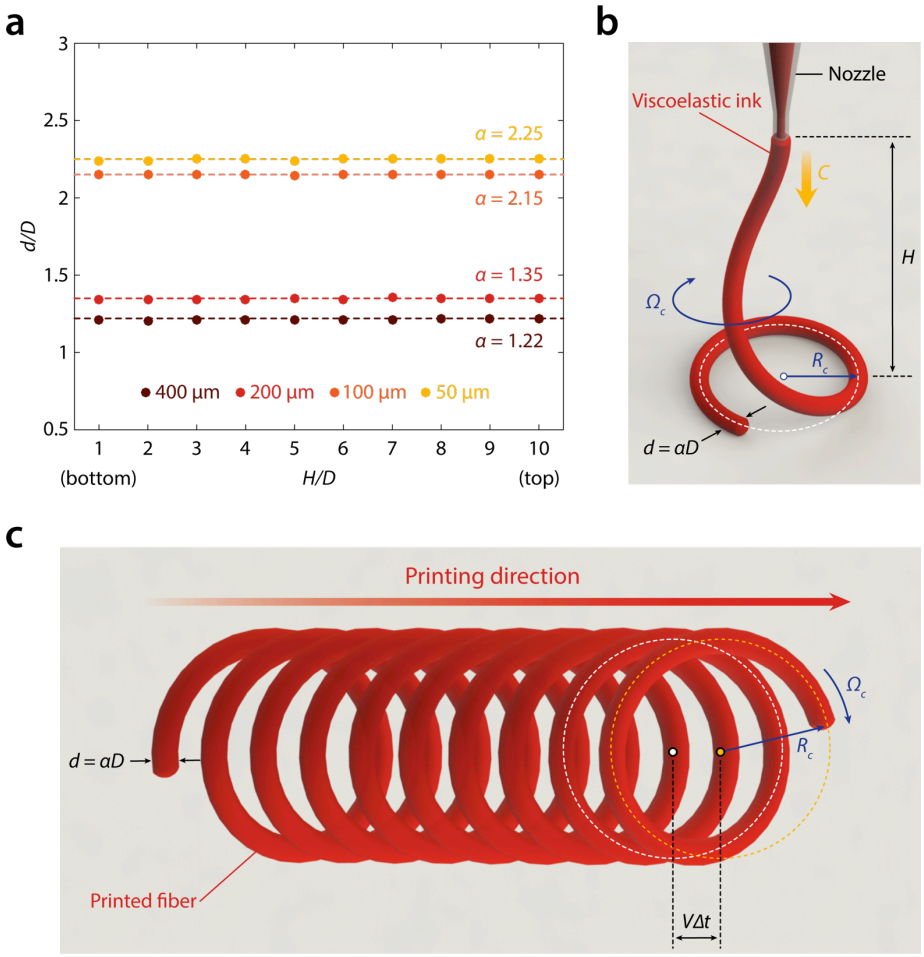

Figure S2. Steady coiling and accumulation of viscoelastic ink printing. a) Plot of d/D as a function of H/D for various nozzle sizes. Dots represent experimental data, and the dotted lines represent corresponding α for each nozzle. b) Schematic illustration for the steady coiling of viscoelastic inks. When the gravitational stretching of viscoelastic inks is negligible, the steady coiling speed becomes the same as the ink feed speed, $U_c = C$, providing the printed fiber diameter in coiling instability as $d = \alpha D$. c) Schematic illustration for the accumulation mode by the overlapping of printed fibers. When $V\Delta t$ is smaller than αD, the printed fibers merge to form a thickened fiber, giving the accumulation mode of printing.

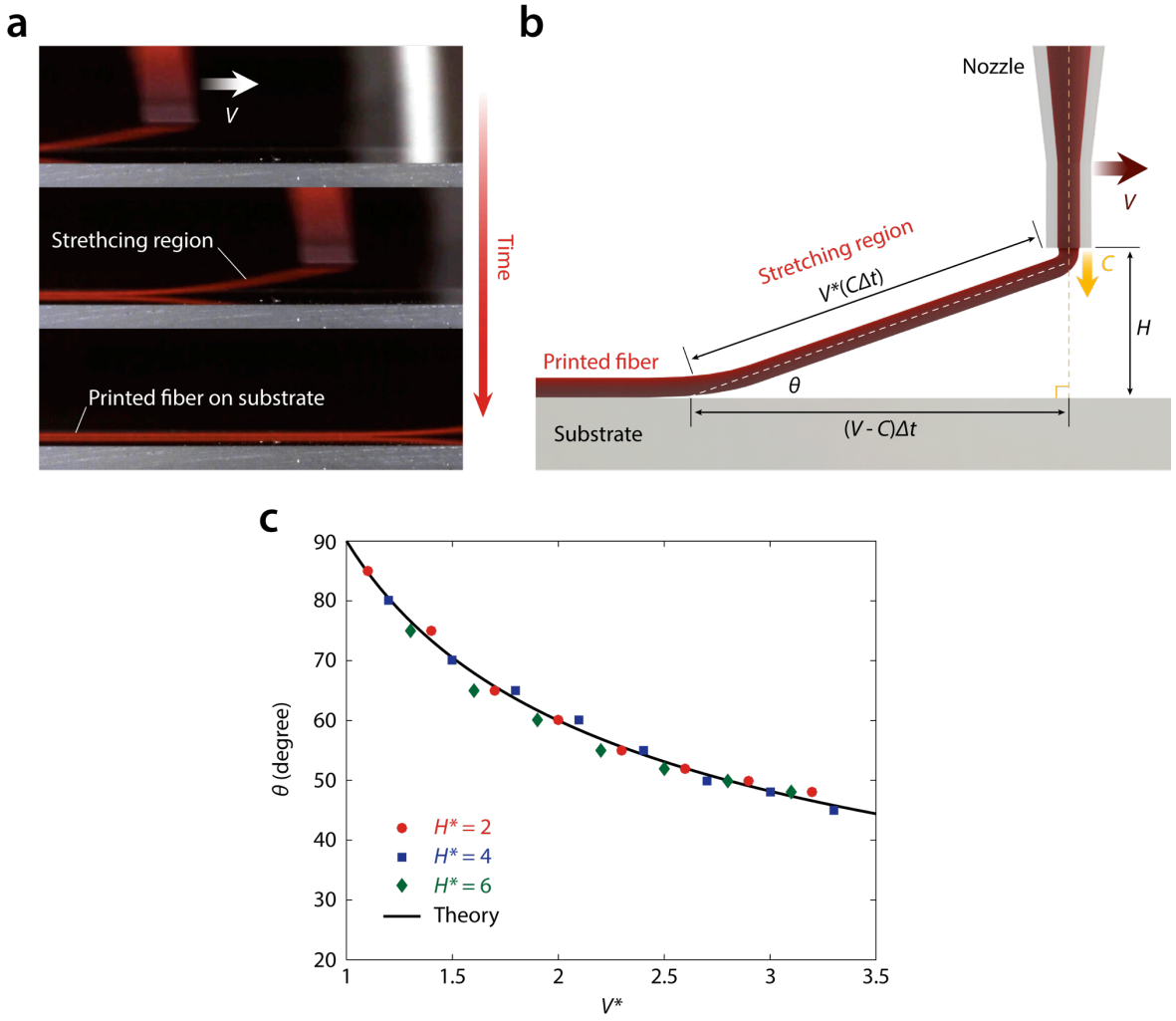

Figure S3. Stretching mode in DIW 3D printing of viscoelastic ink. a) Time-lapse images of a stretching region of the printed viscoelastic ink for V^* >1. b) Schematic illustration for the stretching mode with corresponding geometric parameters. c) Plot of stretching angle θ as a function of V^* for various H^*. Dots represent experimental data, and the solid curve represents the theoretical prediction.

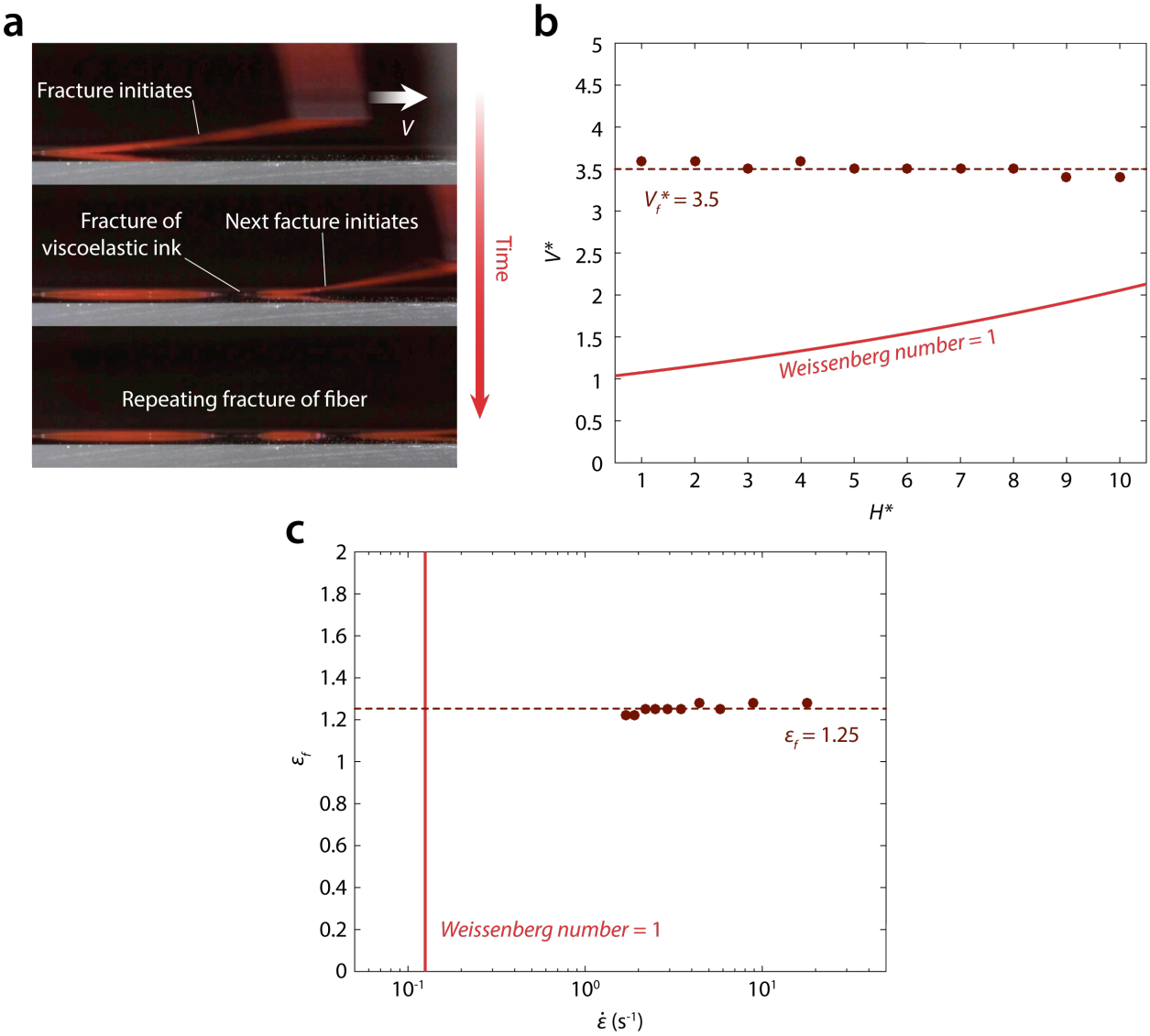

Figure S4. Discontinuous mode in DIW 3D printing of viscoelastic ink. a) Time-lapse images of fracture of the printed fiber for $V^* > V_f^*$. b) Plot of experimentally measured V^* for the onset of fracture failure as a function of H^*. Dots represent experimental data, and the dotted line represents corresponding V_f^*. The solid line represents the values of V^* above which $Wi > 1$. c) Plot of true strain rate $\dot{\varepsilon}$ as a function of true strain at fracture ε_f. The solid line represents the value of $\dot{\varepsilon}$ above which $Wi > 1$.

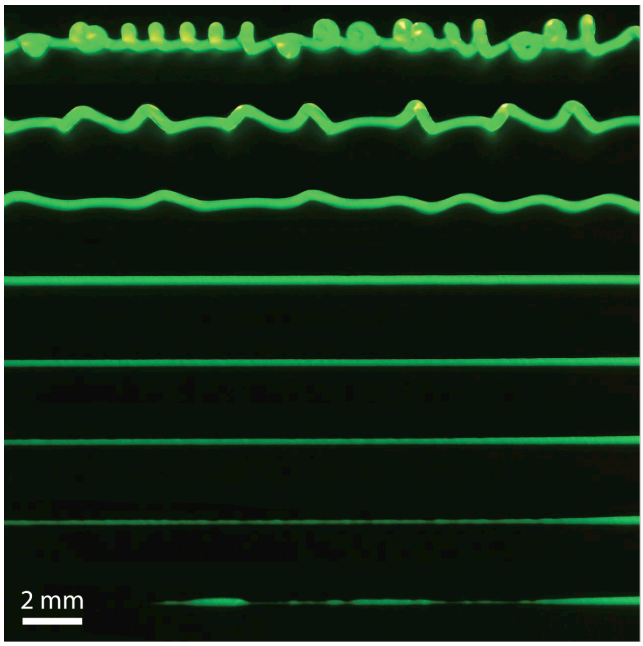

Figure S5. Phase diagram assisted printing of various modes of DIW 3D printing for the hydrogel ink (PEO solution). The new strategy of DIW 3D printing is applicable for a wide range of viscoelastic inks while boundaries for each mode depend upon material properties.

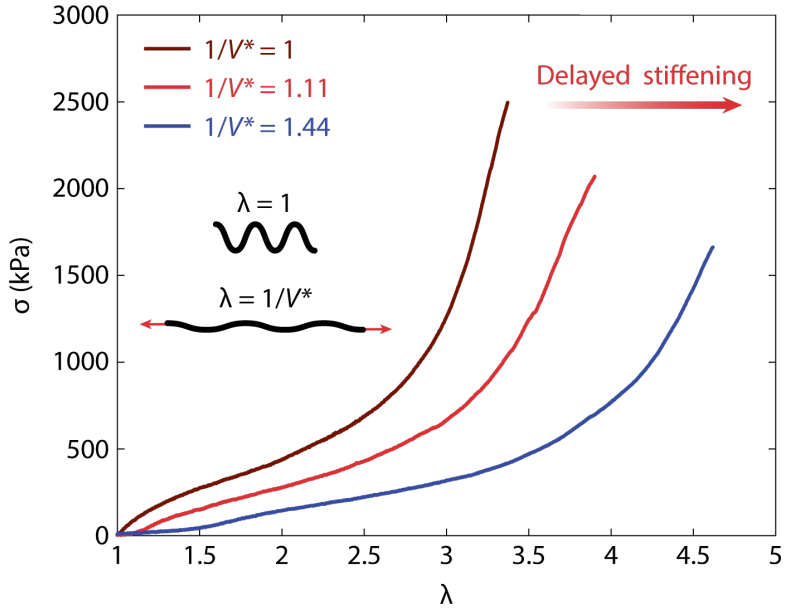

Figure S6. Plot of nominal stress σ as a function of stretch λ of printed fibers under tension. Delayed stiffening happens under tension due to initial stretching of the meandering patterns with low resistance. The delayed stiffening is highly tunable by selecting appropriate printing parameters based on the phase diagram.

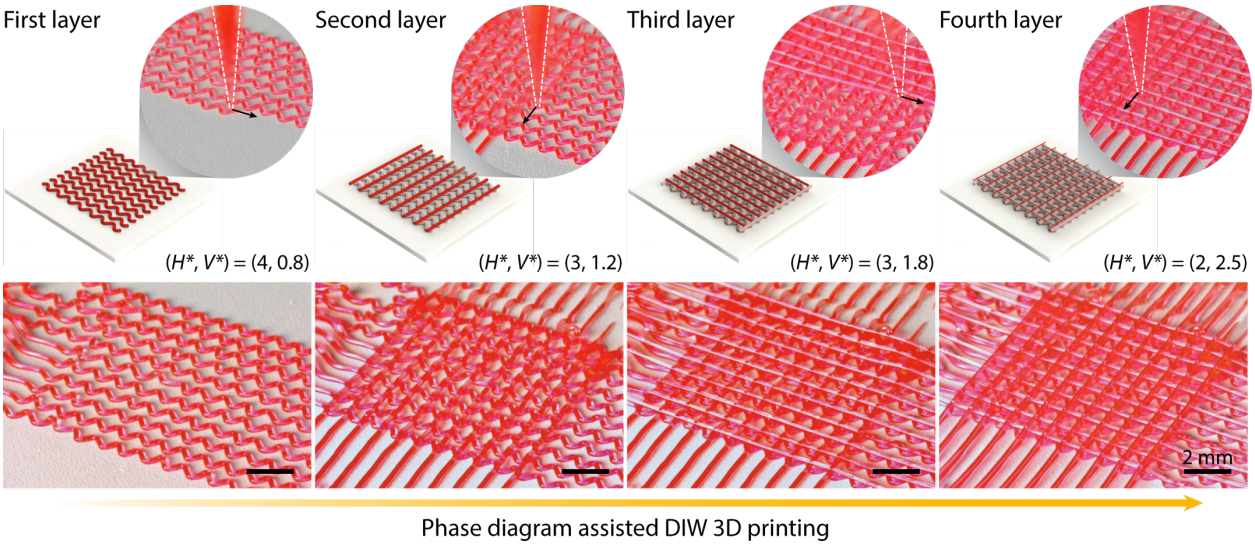

Figure S7. Phase diagram assisted printing of 3D structure with different modes for each layer. Various geometries and sizes of fibers can be printed by a single nozzle without change in nozzle or ink during printing processes.

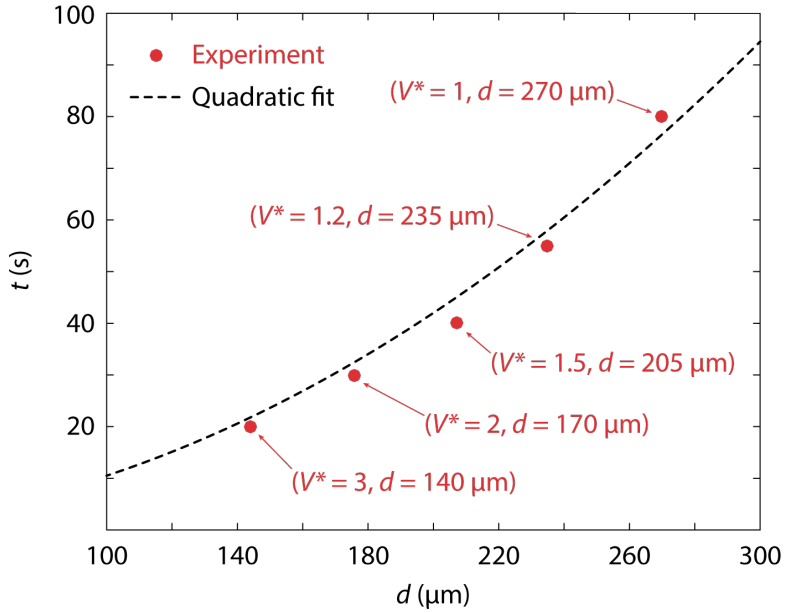

Figure S8. Plot of equilibrium swelling time t as a function of printed fiber diameter d in solvent. Printed fibers with various sizes exhibit gradient in swelling responses in THF. Dots represent experimental data, and the dotted curve represents the quadratic diffusion relation, $t \sim d^2$.

Video S1

Various modes of DIW 3D printing at $H^* = 5$. The corresponding printing parameters are shown in the phase diagram.

Video S2

DIW 3D printing of solid structures with varying fiber diameters by continuous single nozzle printing sequences.

Video S3

DIW 3D printing of a multi-layered structure with different modes at each layer. The corresponding printing parameters are shown in the phase diagram.

Video S4

DIW 3D printing of a multi-layered mesh structure with varying fiber diameters by a single nozzle.

Video S5

Swelling of a gradient 3D structure in THF. Difference in swelling time scales due to gradient fiber diameters gives initial inhomogeneous swelling followed by equilibration in fully swollen state.